Nuclear Physics A533 (1991) 601–616
North-Holland

NUCLEAR PHYSICS A

SPIN-DEPENDENT NEUTRON–PROTON TOTAL CROSS SECTION DIFFERENCES $\Delta\sigma_L$ AND $\Delta\sigma_T$ FROM 140 TO 590 MeV

R. BINZ[1], B. VAN DEN BRANDT[2], R. BÜCHLE[1], M. DAUM[2], Ph. DEMIERRE[3], J. FRANZ[1], G. GAILLARD[3], N. HAMANN[1], R. HESS[3], J.A. KONTER[2], F. LEHAR[4], C. LECHANOINE-LELUC[3], S. MANGO[2], R. PESCHINA[1], F. PERROT-KUNNE[4], D. RAPIN[3], E. RÖSSLE[1], P.A. SCHMELZBACH[2], H. SCHMITT[1] and R. TODENHAGEN[1]

[1] *Fakultät für Physik der Universität Freiburg, D-7800 Freiburg, Germany*
[2] *PSI, Paul Scherrer Institut (formerly SIN), CH-5234 Villigen, Switzerland*
[3] *DPNC Université de Genève, CH-1211 Genève 4, Switzerland*
[4] *DPhPE/SEPh, CEN-Saclay, F-91191 Gif-sur-Yvette, France*

Received 10 December 1990

Abstract: A polarized neutron beam at PSI has been used to measure the spin-dependent neutron-proton total cross sections $\Delta\sigma_L$ and $\Delta\sigma_T$ from 140 to 590 MeV. The results are compared with recent phase-shift calculations.

E | NUCLEAR REACTION ^{1}H (polarized n, n), E = 140–590 MeV; measured longitudinal, transverse σ differences. Transmission method.

1. Introduction

For a complete description of the nucleon–nucleon interaction it is necessary to study both proton–proton and neutron–proton systems, in order to get information on the isoscalar part of the interaction. In contrast to the situation for the pp data, the experimental information on neutron–proton scattering is still rather poor [1,2]). This is due to the difficulties in setting up a polarized neutron beam. Only recently has the situation begun to change and one can expect more high-precision np polarization data in the near future, in particular from PSI, where a new polarized neutron beam facility is under construction [3]). A polarized neutron beam has successfully been set up in the nE1 beam line at PSI [4–7]), and was used for a series of polarization experiments. In the present paper we report on measurements of the spin-dependent total cross section differences $\Delta\sigma_L$(np) and $\Delta\sigma_T$(np).

2. Formalism

The nucleon–nucleon total cross section can be written as [8])

$$\sigma_{tot} = \sigma_{0,tot} + \sigma_{1,tot}(\boldsymbol{P}_b\boldsymbol{P}_t) + \sigma_{2,tot}(\boldsymbol{P}_b\boldsymbol{k})(\boldsymbol{P}_t\boldsymbol{k}) , \quad (1)$$

where P_b and P_t are the polarization vectors of beam and target, respectively, and k is a unit vector in the beam direction. The unpolarized total cross section $\sigma_{0,\mathrm{tot}}$ has been measured for the neutron-proton system with high precision [9,10]. The two other cross sections are related to the observables $\Delta\sigma_L$ and $\Delta\sigma_T$ by

$$\Delta\sigma_L = \sigma(\rightleftarrows) - \sigma(\rightrightarrows) = -2(\sigma_{1,\mathrm{tot}} + \sigma_{2,\mathrm{tot}}), \tag{2}$$

$$\Delta\sigma_T = \sigma(\downarrow\uparrow) - \sigma(\uparrow\uparrow) = -2\sigma_{1,\mathrm{tot}}, \tag{3}$$

where $\Delta\sigma_L$ and $\Delta\sigma_T$ are the cross section differences measured with beam and target polarization vectors parallel and antiparallel to each other, and oriented longitudinally ($\Delta\sigma_L$) or transversally ($\Delta\sigma_T$) with respect to the beam. The isoscalar ($I = 0$) parts of $\Delta\sigma_L$ and $\Delta\sigma_T$ can be evaluated according to:

$$\Delta\sigma_{L,T}(I=0) = 2\Delta\sigma_{L,T}(\mathrm{np}) - \Delta\sigma_{L,T}(\mathrm{pp}). \tag{4}$$

Each isospin channel can be further separated into spin singlet and triplet parts:

$$\sigma_s = \sigma_{0,\mathrm{tot}} - 3\sigma_{1,\mathrm{tot}} - \sigma_{2,\mathrm{tot}}, \tag{5}$$

$$\sigma_{t,0} = \sigma_{0,\mathrm{tot}} + \sigma_{1,\mathrm{tot}} - \sigma_{2,\mathrm{tot}}, \tag{6}$$

$$\sigma_{t,\pm 1} = \sigma_{0,\mathrm{tot}} + \sigma_{1,\mathrm{tot}} + \sigma_{2,\mathrm{tot}}. \tag{7}$$

3. The polarized neutron beam

3.1. THE NEUTRON BEAM AT PSI

The experiments were performed at the SIN/PSI nE1 beam. Neutrons were produced by quasifree elastic and inelastic C(p, n)X processes, with 590 MeV protons incident on a 6 cm thick carbon target (target E). Neutrons emitted at an angle of 3.4° were collimated to form a beam, which had a cross section of about 1×1 cm^2 at a distance of 20 m from the production target, where the polarized target was placed. The energy spectrum of the beam was continuous, with a quasielastic peak at 535 MeV [ref. [11])]. The accelerator was operated in the so-called 17 MHz mode by suppressing two out of three successive bunches. This gives a time separation of the proton bunches on the production target of 59.25 ns, which enables an unambiguous determination of the neutron energy by time-of-flight technique for all energies above 120 MeV.

Polarized neutrons were obtained using longitudinally polarized protons incident on target E (see sect. 3.3). The neutron polarization could be subsequently precessed by means of a dipole magnet.

3.2. THE POLARIZED ION SOURCE

The ion source for the polarized proton beam is of the atomic beam type [12,13]. Nuclear polarization is generated by a set of strong and weak field rf-transitions. Selection of a particular polarization is achieved by switching on or off the rf-power

of the corresponding transition unit, which can be done up to a maximum frequency of 100 Hz. In this experiment the sign of the polarization was reversed every second. Correlations between polarization and beam parameters, such as intensity, phase space, etc. are negligible for these experiments [14]).

The beam is extracted from the ionizer and is injected for acceleration into two successive cyclotrons with end energies of 72 MeV (injector cyclotron) and 590 MeV (ring cyclotron), respectively. After the extraction of the protons into the PSI external proton channel the polarization vector of the protons is turned into the longitudinal direction. This is achieved by first turning it around the beam axis from the vertical into the horizontal plane by a superconducting solenoid of 2.26 teslameter strength. Behind the solenoid the proton beam is deflected by 32.5° in order to bring it into its final direction towards the target E. By this deflection the spins of the protons are precessed so that their direction differs from the beam axis by only 5°. The intensities of the polarized proton beam at the various stages of the system are given in table 1.

3.3. SPIN TRANSFER ON CARBON

The polarization of the produced neutrons, P_n, is longitudinal, resulting from longitudinal polarization transfer on carbon, which has been investigated in a recent experiment [7]). This transfer mechanism gives sufficiently high neutron polarizations over a large neutron energy region, and has the great advantage, that the standard production target E can be used. The transversal components of the neutron polarization, emerging from $K_{0s''k0}$ (notation as in ref. [8])), and possibly from a small vertical component of the incident proton beam are small. Obviously, they do not contribute at all to the $\Delta\sigma_L$ measurement. For the $\Delta\sigma_T$ measurement, the neutron spin is precessed from longitudinal to vertical direction, leaving small horizontal components of the neutron polarization. Again, these components do not contribute, since here the target polarization is vertical. In the present experiment the average polarization of the protons incident on target E was $P_p = 0.85 \pm 0.02$. The neutron polarization P_n achieved with this proton beam is shown in fig. 1 as a function of the neutron energy. Its value changes from $P_n \sim -0.3$ at 300 MeV to $P_n \sim -0.45$ above 400 MeV. The neutron polarization was continuously measured with two independent polarimeters [7]), placed behind the $\Delta\sigma$ experiment at a distance of 61 m

TABLE 1

Intensities of the PSI polarized proton beam

Atomic beam into ionizer	5×10^{16} atoms/s
Beam current from ionizer	300 μA
Beam current at injection (13.5 keV)	45 μA
Beam current after first acceleration stage (72 MeV)	3-6 μA
Beam current after second acceleration stage (590 MeV)	3-5 μA

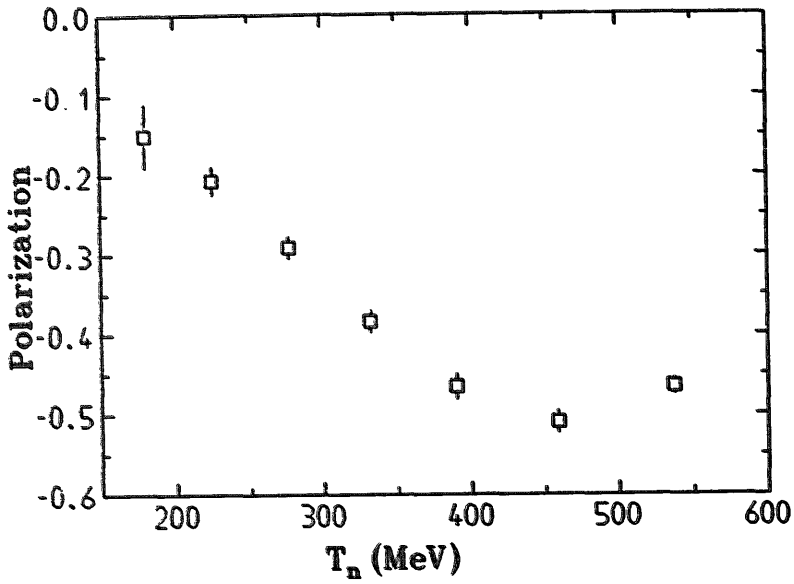

Fig. 1. Longitudinal polarization P_n of the neutron beam as a function of the neutron energy.

from target E. By these polarimeters the asymmetry of the free neutron–proton scattering on hydrogen was used to measure the neutron beam polarization as a function of the energy. For the analysis of these measurements the np analyzing power A_{00n0} is needed as input. Thus the resulting neutron beam polarization P_n depends on the knowledge of the analyzing power. We have used values calculated from a recent Saclay–Geneva phase-shift analysis [15]). More details are given in the appendix.

4. The polarized proton target

The polarized proton target consisted of frozen beads of porphyrexide doped butanol, $CH_3(CH_2)_2CH_2OH$, immersed in liquid ^3He at a temperature of about 0.5 K in a thin-walled, horizontally positioned copper cylinder 2 cm in diameter. For the $\Delta\sigma_L$ measurement, the target was 15 cm long and was placed in the magnetic field of a 2.5 T horizontal solenoid. For the $\Delta\sigma_T$ measurement the target was 12 cm long and was placed between the poles of a C-magnet. For both measurements, the copper cell was carefully aligned, so that the cylinder axis coincided with the neutron beam axis. The sample was polarized by the method of dynamic nuclear orientation. The target polarization was continuously monitored by NMR technique. Calibration was done using the thermal equilibrium polarization signal. Typical polarizations obtained during the experiments were $P_t \sim 0.55$ for $\Delta\sigma_L$ and $P_t \sim 0.62$ for $\Delta\sigma_T$, with an uncertainty of $\Delta P_t = \pm 0.02$. At the end of the experiments, the target material was melted and weighed under nitrogen atmosphere. The estimated error of this weight measurement introduces an uncertainty in the number of protons per mb of the target of $\Delta n_H / n_H = 2.4\%$. For the $\Delta\sigma_T$ measurement an additional systematic

error came from an incomplete filling of the target cell, resulting in a total systematic error of $\Delta n_H/n_H = 12\%$ in this case.

5. Experiment

5.1. SET-UP

The experimental set-up is shown in fig. 2. The spin-dependent cross sections are measured by the attenuation of the beam passing through the polarized proton target (PPT). The neutron intensity before the polarized target was monitored with a scintillator set (M in fig. 2) consisting of a veto counter followed by a CH_2 converter, and two scintillation counters in coincidence for the detection of recoil protons from the converter. Two similar detectors (S and T in fig. 2) were used to measure the neutron intensity behind the absorber. The last scintillator of S served also as a veto for T.

In order to determine $\Delta\sigma$ as a function of the incident neutron energy, the neutron time-of-flight (t.o.f.) was measured between the target E and the detectors behind the PPT, using the 17 MHz rf-signal of the cyclotron, i.e. over a range of 59.25 ns. A 2 cm thick copper absorber between S1 and S2 (and correspondingly T1 and T2) suppressed recoil protons from neutrons with energies below 130 MeV, which would fall in the same t.o.f. range, modulo 59.25 ns. In this way an unambiguous determination of the neutron energy above this value was achieved.

For the $\Delta\sigma_T$ measurement a transverse neutron polarization is needed. Therefore the neutrons passed a magnet (AHG) with horizontal field, oriented perpendicular

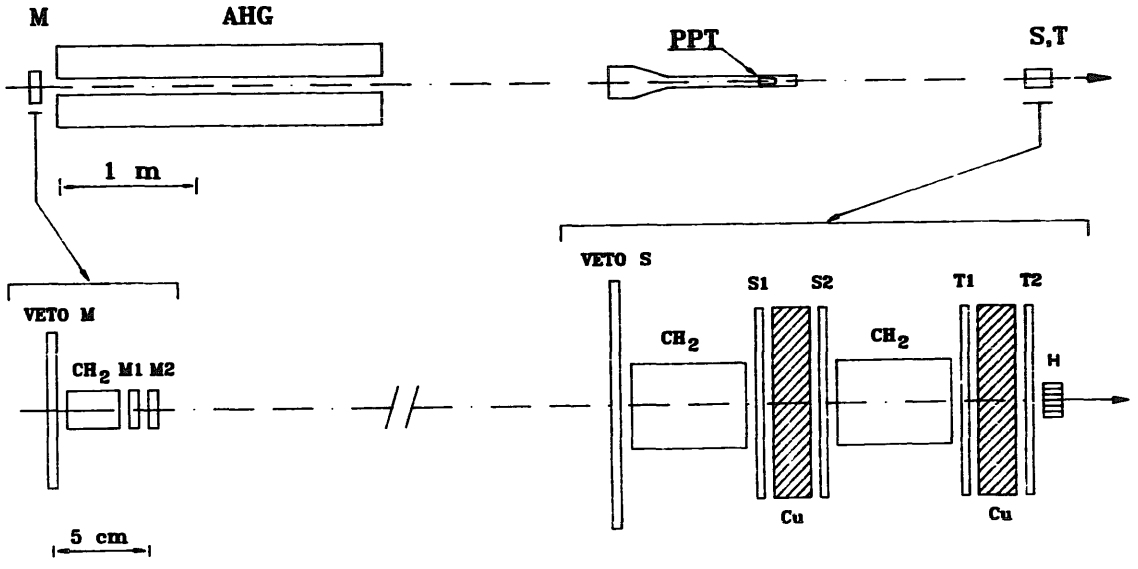

Fig. 2. Experimental set-up. AHG: spin precessing magnet; PPT: polarized proton target; M, S, T: beam intensity monitors; Veto M, M1, M2, Veto S, S1, S2, T1, T2: scintillation counters; H: beam position hodoscope; Cu: copper absorber; CH_2: polyethylene converters; the target magnets (solenoid for $\Delta\sigma_L$, C-magnet for $\Delta\sigma_T$) are not shown.

to the beam. The effective field length was 1.94 m, and the field was set to 1.01 T, in order to rotate the spin of 500 MeV neutrons by 90°. At other energies an appropriate correction has been applied.

A hodoscope (H in fig. 2), consisting of six scintillators of 3 mm width each, and 10 mm thickness, was positioned behind the T monitor. It allowed to monitor the centre of the beam intensity to better than 0.1 mm.

During our experiments, the proton beam intensity was typically 3 μA on the production target. The neutron intensity was about 10^5 neutrons/(μA · s) above 200 MeV.

Before this set-up was completely installed, a test run with only half of the transmission detector, a rather simple electronics, and a 1.2 cm thick polarized target was performed, yielding four additional points for $\Delta\sigma_T$, with rather large errors. These data are not included here. They have been presented elsewhere [16]).

5.2. ELECTRONICS AND DATA ACQUISITION

Due to the small target thickness, the counting rate differences to be measured are small, and therefore high statistics are needed. In a data acquisition system in which TDCs are used to digitize the measured time-of-flight, the event rate is limited to a few hundred per second, and very long beam periods would be needed to achieve a reasonable statistical error. Therefore a different method was applied. The scheme of the electronics is shown in fig. 3 for the S detector. A similar circuit was used for the T detector. The energy range between 140 and 590 MeV was divided

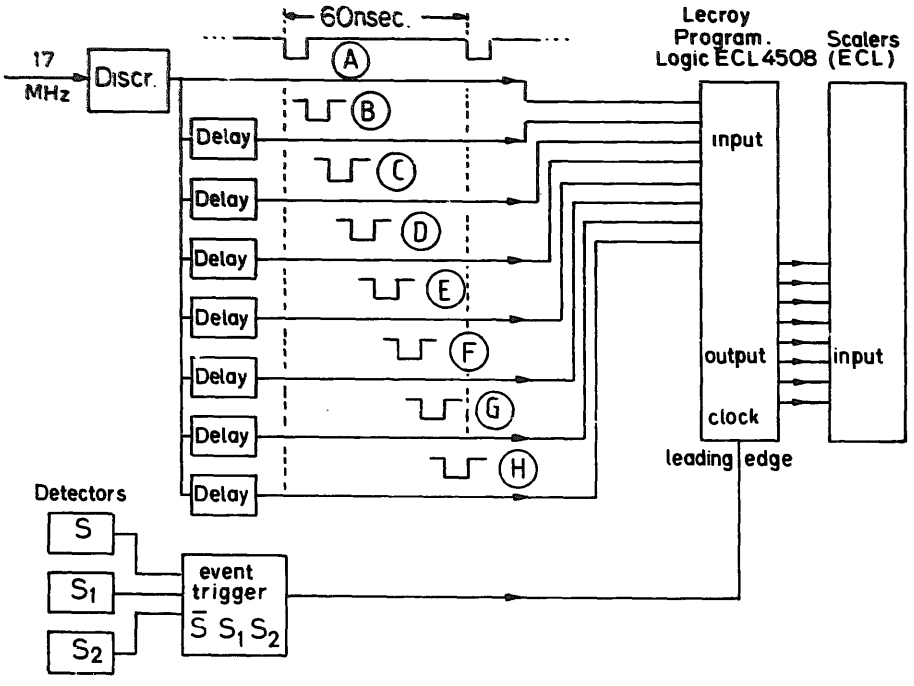

Fig. 3. Schematic diagram of the electronics for the $\Delta\sigma$ measurements.

into seven energy bins, using seven non-overlapping time-of-flight windows, which were selected by appropriately delayed pulses from the 17 MHz signal in coincidence with the event signal. Another time window, of 3.5 ns width, was set, covering the border region between the high and the low end of our energy range, where within our time resolution of 2.2 ns no clear energy determination is possible, due to the 59.25 ns ambiguity. The count rate of this bin is very sensitive to time shifts and can therefore be used to control the stability of the electronics.

Coincidences with the event signal were made in a rather sophisticated way with a LeCroy ECL-module PLU 4508, a programmable coincidence unit which works on the principle of a fast look-up table. This was necessary in order to prevent the problem of double counting in two adjacent bins, or of not-counting, if the bin width is changing due to a drift in the electronics. The timing diagram of the pulses and the corresponding definition of the t.o.f. bins 1–8 are shown in fig. 4. The bin number is defined by the front edges of the corresponding pulses A–H. It was insensitive to a variation of the pulse widths, i.e. the rear edges within ±2 ns. The widths of the pulses A–H are given in the left-hand table of fig. 4. The definition of the bins is shown in the right-hand table of the figure, where "1" and "0" means, that the signal is required, or must be absent, respectively, and "X" means that

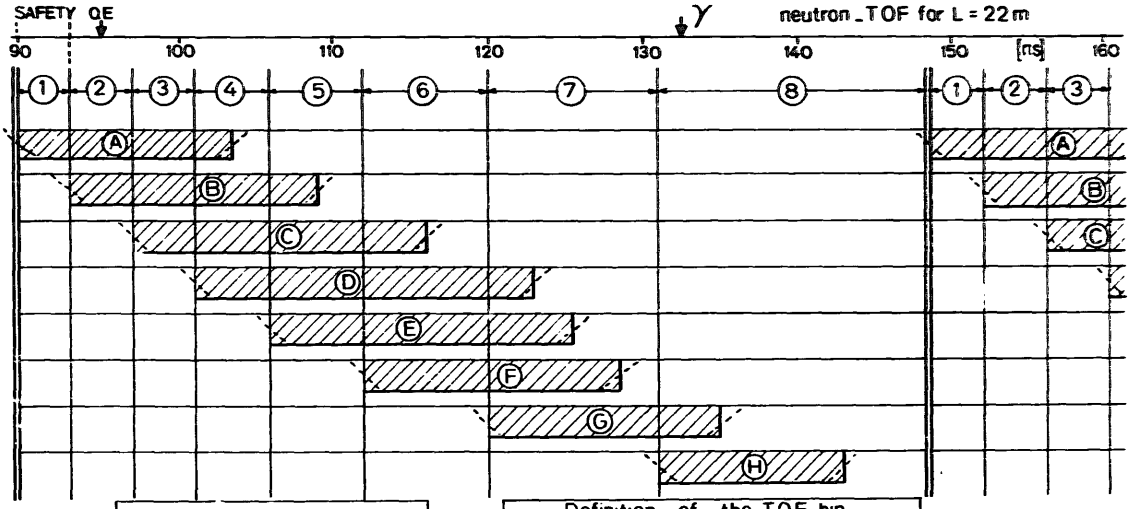

Pulse	width.
A = 14 ns ±1	E = 19.5 ns ±1
B = 16 ns ±1.5	F = 16.5 ns ±1
C = 19 ns ±2	G = 15 ns ±2
D = 22 ns ±1	H = 12 ns ±2

Definition of the TOF bin			
bin	HGFEDCBA	bin	HGFEDCBA
1	00000001	6	0011 1X00
2	00000011		
3	000001 1X	7	0111X000 011X0000 01X00000
4	00001 11X		
5	0001 11X0	8	1X000000 00000000

Fig. 4. Timing diagram of the electronics defining the t.o.f. windows. The shadowed areas are the overlapping pulses. In the right-hand table, the definitions for the bins 1–8 are given. The widths of the pulses A–H are shown in the left-hand table. On the top of the diagram, the time-of-flight between the target E and the S detector is indicated for the quasielastic neutrons, and for the photons from the π^0 decays, which is used for the t.o.f. calibration.

either of these conditions is accepted. Bin 1 is the above mentioned control bin. Bin 2 contains the quasielastic peak, and the following ones have increasing widths, corresponding to nearly equal energy widths (see tables 2 and 3 for details). The absolute range of the windows have been adjusted using the time-of-flight of photons from the π^0 decays at the target E. The position of the γ-peak and of the quasielastic peak (535 MeV) are also indicated in fig. 4.

The output signals of the PLU were alternately accumulated in two groups of eight scalers, according to the orientation of the beam polarization, which was changed every second. Most of the electronics was realized with ECLine modules and was controlled by a PC through a CAMAC system. Every 20 min the contents of the scalers were written on disc, together with the actual values of the beam and target polarizations (see also sect. 5.3).

A total event rate of ~3500/s was achieved from S and T together. For the M detector in front of the target, monitoring the intensity of the incident beam, only the energy integrated rates M^+ and M^- were needed.

5.3. STABILITY TESTS

Great care has been devoted to possible time shifts in the electronics, which could lead to a shift in the energy ranges defined by the time windows. Moreover, since the t.o.f. of the incident neutrons is known only modulo 59.25 ns, such a shift could bring low energy neutrons into the "higher energy" window. Therefore, as described in the previous section, the additional time window was set covering the border region between high and lower energy. Its count rate, being very sensitive to shifts in the electronics, was used to control the stability of the window setting. It was checked regularly during the run, and corrections were applied whenever necessary.

An asymmetry error can occur, if the beam position varies with time, or if it depends on the beam polarization state. This was permanently controlled with the above-mentioned beam hodoscope (sect. 5.1). No beam-polarization-dependent effect was observed within the limits of 0.1 mm. Also, no time-dependent shift of the beam position was observed during the measurement.

As discussed in sect. 3.3 the neutron beam polarization was measured simultaneously with hydrogen polarimeters. In addition, the stability of the polarization of the proton and the neutron beams were continuously monitored:

(i) In front of the solenoid a small fraction of the vertically polarized proton beam was split off into another beam line, and scattered on a carbon target. The asymmetry measured at 12°, being about 0.3, was recorded.

(ii) For the neutron polarization, a small polarimeter, measuring the left–right asymmetry of the recoil particles at ±30° from a CH_2 target, was mounted behind the $\Delta\sigma$ set-up, in order to monitor the energy averaged neutron polarization.

Both polarization monitors were recorded together with the $\Delta\sigma$ scalers, and no sizeable change of polarization was observed during data taking.

6. Data analysis

6.1. TOTAL CROSS SECTIONS

The total cross section difference is given by [17]:

$$\Delta\sigma = \frac{1}{(P_n P_t n_H)} \ln\left[\frac{S^+ M^-}{M^+ S^-}\right]. \tag{8}$$

Here P_n and P_t are the beam and target polarizations, n_H is the target thickness (protons/mb), and S^+/M^+, S^-/M^- are the normalized S detector rates for parallel and antiparallel spin, respectively. A similar relation holds for the T detector. The calculation of the cross sections from the data according to eq. (8) is straightforward. The beam and target polarizations P_n and P_t were evaluated from the simultaneously recorded data of the polarimeter and of the target, respectively. However, n_H being rather small ($\sim 7\times 10^{-4}$/mb), the effect we measure, $\ln[(S^+M^-)/(M^+S^-)]$, is only $0.2\text{–}2\times 10^{-3}$. Therefore, small effects caused by an imperfect alignment of the set-up can be important. This is discussed in the next section.

6.2. DISPLACEMENT EFFECTS

The precision of the geometrical adjustment of the detectors is very important, especially for the $\Delta\sigma_T$ measurements, where a small displacement Δx can introduce large asymmetries through a dependence of S and T rates on the beam polarization. This effect has been discussed for proton-proton scattering at 800 MeV in ref. [17]). Therein, it was found that a displacement of the order of $\Delta x = \pm 2.5$ mm and a distance $L = 1100$ mm between target and detector had no influence on $\Delta\sigma_T$. We refer to this paper, retaining the limit of $\Delta x = 2.5$ mm, for the discussion of the neutron-proton scattering.

We discuss first the measurement of $\Delta\sigma_T$. The effects produced by a displacement of the PPT and of the transmission detector or of its elements with respect to the beam axis are of the same order of magnitude as in the pp case, as far as the scattering on the PPT alone is concerned. But in contrast to the pp case, where the target is the only scatterer, we have in the np case a second scatterer - the radiator of the detector. This is illustrated in fig. 5 where the transmission detector is moved out of the beam axis by Δx. The distance between the PPT and the detectors S and T is $L \sim 2000$ mm, whereas the average distance between the CH_2 scatterers and the corresponding S or T scintillators is only $l = 60$ mm. The difference in the effective scattering angles θ_{lab} for a scattering on the CH_2 in the detector, caused by Δx is by the ratio L/l larger than the corresponding effect due to scattering on the PPT. Therefore, a displacement of the order of $\Delta x = \pm 2.5$ mm will produce in our case an asymmetry which is by a factor $L/l \sim 30$ times larger than the asymmetry caused by scattering on the PTT.

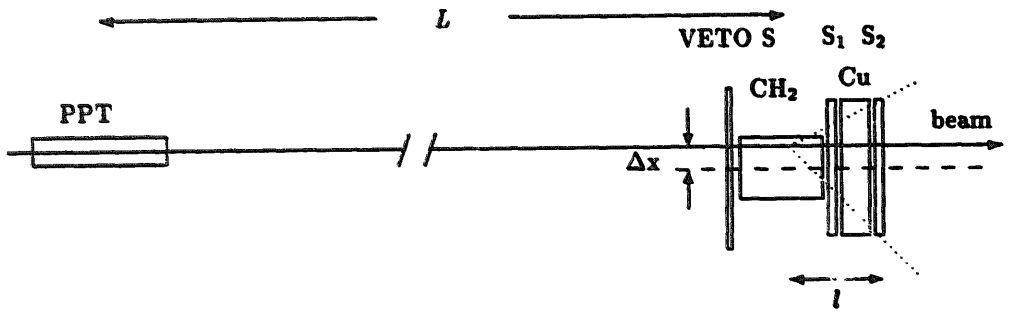

Fig. 5. Illustration of the effect, caused by a perpendicular displacement Δx of the S detector with respect to the beam. The distance between PTT and the detector, $L = 2000$ mm, is relevant for the scattering on the target; the corresponding distance for scattering on the radiator is $l = 60$ mm. The meaning of the other symbols is the same as in fig. 2.

Consequently, in order to minimize these effects to a negligible level, the alignment of the set-up with respect to the beam would have to be done with a precision of 2.5 mm/30 ~ 0.08 mm, which is not feasible. However, the displacement effects are practically independent of the PPT-polarization, whereas $\Delta\sigma_T$ changes its sign with P_t. Therefore, the sign of the target polarization was changed every day, and by unweighted averaging the results (with appropriate sign) from the two target polarities the displacement errors cancel.

For the $\Delta\sigma_L$ measurements, these effects are less important, but small residual components of the neutron polarization in transverse directions can also lead to asymmetries if the alignment of the detectors is not perfect. Again, this was compensated by measuring with both target polarities.

In a similar way such effects can also appear if the monitor M in front of the spin precession magnet AHG is displaced, but this is also compensated, if both target polarities are used. In the $\Delta\sigma_T$ measurement, where the AHG is used for spin rotation, an asymmetry on M could be introduced by the fringe field of this magnet. Therefore, also the polarity of the AHG was changed several times.

7. Results

The results obtained for $\Delta\sigma_L$ and $\Delta\sigma_T$ are given in tables 2 and 3. In column 2, only the statistical errors are given. These errors are due to the counting rates of the S and T detectors and contain also the statistical errors of the beam polarization.

There is also a statistical error from the monitor rate M, which is common to all data points, since M is an integral monitor. Therefore this error, though statistical in nature, acts like a common systematic error to all data points. The corresponding errors for $\Delta\sigma_L$ and $\Delta\sigma_T$ depend on the energy due to the energy dependence of P_n (see eq. (8)). They are given in column 4.

The errors from the target thickness n_H and the target polarization (see sect. 4) are listed in columns 5 and 6. The quadratic sum of columns 4–6 is given in column 3.

TABLE 2

Spin-dependent np total cross section differences $\Delta\sigma_L$

Neutron energy (MeV) (1)	$\Delta\sigma_L$ (mb) (2)	Systematic errors (mb) (3)	(4)	(5)	(6)	Δt (ns) (7)	ΔT_n (MeV) (8)
537	−7.9 ± 0.6	±0.5	0.4	0.2	0.3	4	110
459	−9.1 ± 0.8	±0.6	0.4	0.2	0.4	4	69
390	−14.8 ± 1.0	±0.8	0.4	0.4	0.6	5	60
332	−17.9 ± 1.8	±0.9	0.5	0.4	0.7	6	57
277	−22.0 ± 2.7	±1.2	0.7	0.5	0.9	8	56
225	−26.6 ± 3.4	±1.6	1.0	0.6	1.1	11	46
180	−31.1 ± 9.4	±2.0	1.4	0.7	1.2	18	55

The errors in column 2 are the statistical ones, including the statistical errors from the beam polarization measurement. The systematic error contributions from the monitor rate, the target thickness and the target polarization are given in columns 4–6, respectively, and the quadratic sums of them, representing the overall systematic errors, are given in column 3. The widths of the defining t.o.f. windows, given in column 7, result in the energy bin widths of column 8.

These errors should be understood as limits of a normalization error, within which all values can only move up or down together.

If the monitor rate M changes with time during the measurement, the normalization (see eq. (8)) can introduce an asymmetry, which may disturb the measurement. Such an eventual effect was carefully investigated as a function of time. The data have also been evaluated without using M, i.e. with $M^+ = M^-$ in eq. (8). It was found, that the deviation from the results with normalized rates was negligible.

A possible contribution from A_{00nn}, or A_{00kk}, due to the finite solid angle of the detectors was estimated to contribute less than 0.02 mb to the final results, and was therefore neglected.

TABLE 3

Spin-dependent np total cross section differences $\Delta\sigma_T$

Neutron energy (MeV) (1)	$\Delta\sigma_T$ (mb) (2)	Systematic errors (mb) (3)	(4)	(5)	(6)	Δt (ns) (7)	ΔT_n (MeV) (8)
537	11.4 ± 0.8	±1.7	0.8	1.4	0.5	4	110
459	10.9 ± 1.2	±1.5	0.7	1.3	0.4	4	69
390	9.4 ± 1.4	±1.4	0.8	1.1	0.4	5	60
332	6.8 ± 1.6	±1.3	1.0	0.8	0.3	6	57
277	3.8 ± 2.2	±1.5	1.4	0.4	0.2	8	56
225	2.2 ± 4.1	±2.0	2.0	0.3	0.1	11	46
180	−6.9 ± 8.8	±3.1	3.0	0.8	0.3	18	55

The meaning of columns 3–8 is the same as in table 2.

8. Discussion

In fig. 6 the results are shown together with data from other experiments, as well as predictions from recent np phase shift calculations. For $\Delta\sigma_L$, the data point from Saclay [16]) is in perfect agreement with our result. In the overlapping region around 550 MeV our data differ from the ANL data points [18]) which have been evaluated from $\vec{p}\vec{d}$ measurements. For $\Delta\sigma_T$, no data from other laboratories are available below 600 MeV. Also shown are calculations prior to our work from the Saclay-Geneva [19]) and the Arndt [20]) phase-shift analyses (PSA). For $\Delta\sigma_T$, the Saclay-Geneva prediction lies fairly well within the data error bars. For $\Delta\sigma_L$, the agreement

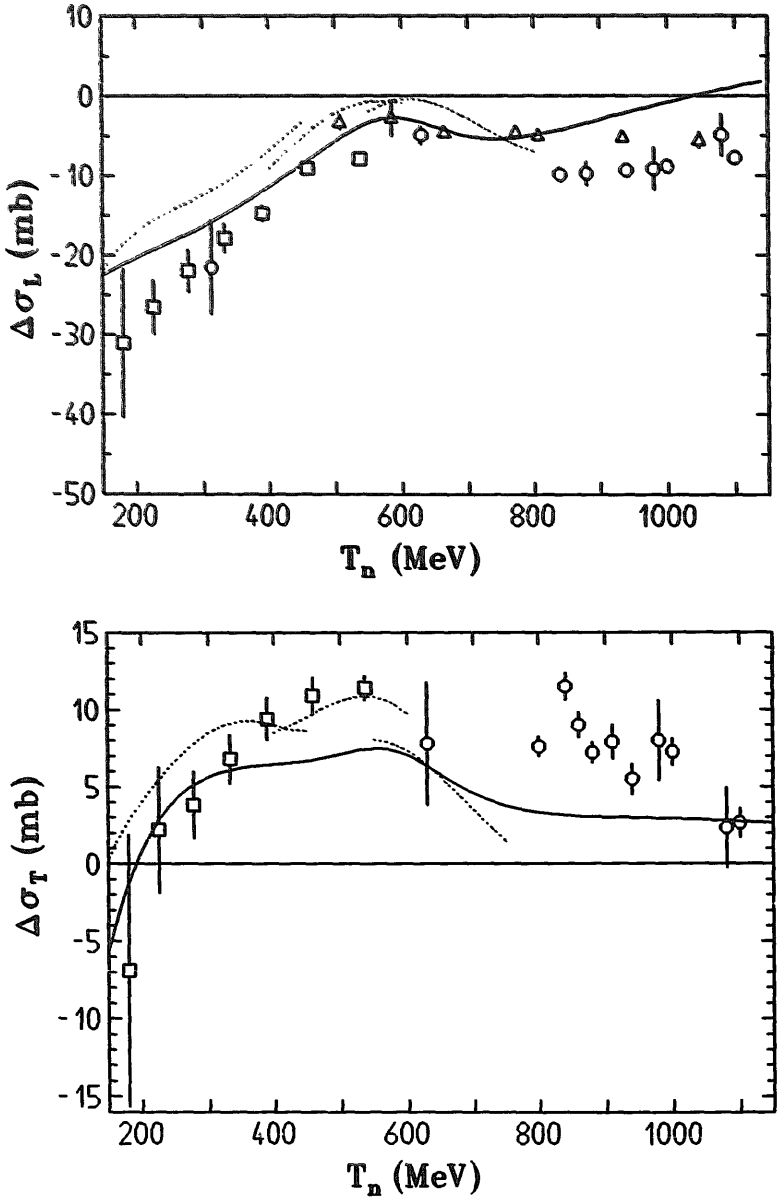

Fig. 6. The spin-dependent np total cross sections $\Delta\sigma_L$ and $\Delta\sigma_T$. □: this work; ○: ref. [16]); △: ref. [18]). The curves are phase-shift predictions: dotted line, ref. [19]); full line, ref. [20]).

with the Saclay-Geneva prediction is worse, due to the fact that the ANL data [18]) have been included in the analysis, in contrast to the Arndt PSA. Using the predictions [20]) for $\Delta\sigma_L$(pp) and $\Delta\sigma_T$(pp), the isoscalar parts of the two cross section differences have been extracted from our data following eq. (4). The results are shown in fig. 7. Here the agreement with both PSA calculations [19,20]) is rather poor.

The experiment benefited from the excellent assistance by many PSI staff members. We acknowledge Dr. Niinikosky from CERN for loaning us the horizontal ^{3}He-cryostat and the C-magnet used for $\Delta\sigma_T$, and the PSI magnet group for the solenoid

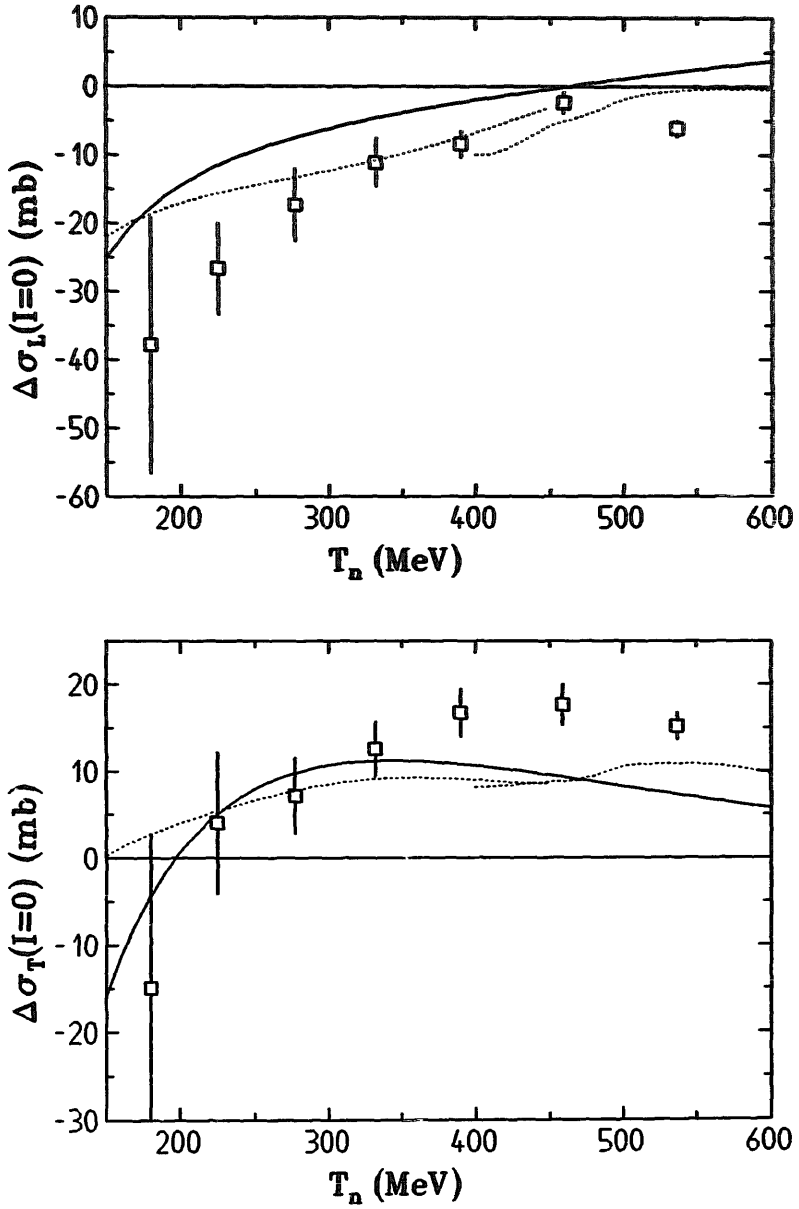

Fig. 7. Isospin $I = 0$ parts of the spin-dependent cross sections. The PSA predictions are from ref. [19]) (dotted line) and ref. [20]) (full line).

used for $\Delta\sigma_L$. This work has been funded by the Federal Minister for Research and Technology (BMFT) under the contract No 0234 FRAI, and the Fonds National Suisse pour la Recherche Scientifique.

Appendix

MEASUREMENT OF THE NEUTRON BEAM POLARIZATION

For the evaluation of the cross section differences $\Delta\sigma_L$ and $\Delta\sigma_T$ the value of the neutron beam polarization is needed. This was measured simultaneously behind the set-up for $\Delta\sigma$ with two different experiments, which determined the asymmetry in free np scattering. In the first one, the neutrons, scattered on a scintillator working as an active target, were detected (method I), while in the second experiment the protons recoiling from a liquid hydrogen target were measured (method II). More details can be found in ref. [7]).

In order to evaluate the neutron polarization from the measured asymmetries, the np analyzing power $A_{00n0}(\theta, T_n)$ has to be known. In method I, the angular region of interest is $10° \leq \theta_{n,c.m.} \leq 30°$, where no experimental information on A is available at our energies. In method II the angular range of the detected protons correspond to $110° \leq \theta_{n,c.m.} \leq 120°$. Here many precise data on A_{00n0} are available, and therefore only the results according to method II have been used.

The events were grouped in 5 MeV wide incident neutron energy bins. For each of these bins, the recoil protons were sorted into 20 angular bins, covering the measured θ range for the protons. For each of these bins, the asymmetry $\varepsilon(\theta, T_n)$ was evaluated,

$$\varepsilon(\theta, T_n) = \frac{N^{\uparrow}(\theta, T_n) - N^{\downarrow}(\theta, T_n)}{N^{\uparrow}(\theta, T_n) + N^{\downarrow}(\theta, T_n)} = P_n(T_n) A_{00n0}(\theta, T_n) . \tag{9}$$

and, from this, the resulting beam polarization $P_n(T_n)$ at the corresponding neutron energy was calculated.

TABLE 4

Polarization of the neutron beam at different energies

Neutron energy (MeV)	$\langle\theta_{n,c.m.}\rangle$	A_{00n0}	P_n
537	110.4	−0.355	−0.466 ± 0.010
459	111.3	−0.289	−0.510 ± 0.014
390	112.1	−0.250	−0.466 ± 0.016
332	112.8	−0.214	−0.384 ± 0.014
277	113.5	−0.190	−0.291 ± 0.014
225	114.1	−0.158	−0.207 ± 0.018
180	114.6	−0.095	−0.151 ± 0.040

The effective analyzing powers A_{00n0} used for the evaluation of P_n are also given.

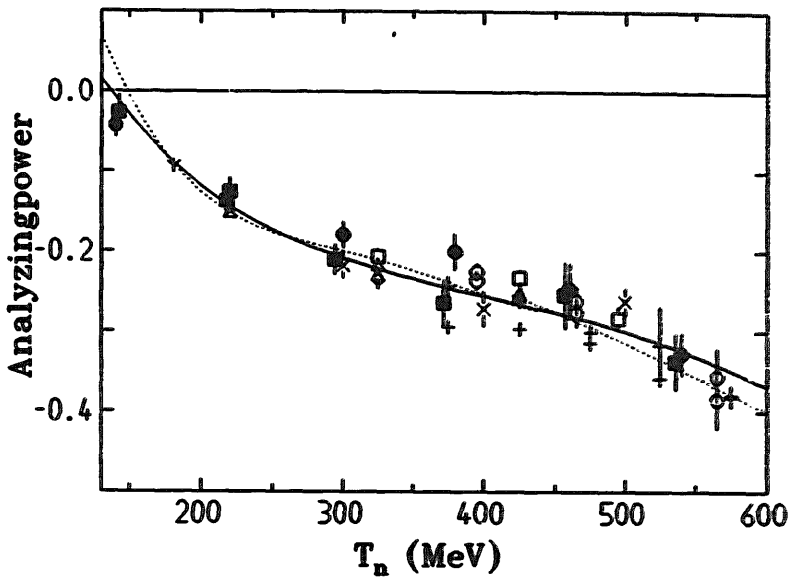

Fig. 8. The np analyzing power used to determine the polarization of the neutron beam. Also shown are values from different experiments taken from the data set of ref. [20]), and unpublished data from PSI (full dots, and full boxes [21])).

The values of $A_{00n0}(\theta, T_n)$ needed for this procedure were obtained from the most recent Saclay–Geneva phase shifts [15]). Average values for the beam polarization have been calculated for the centres of gravity of our energy intervals of the $\Delta\sigma$ measurements. The "effective" averaged angles $\langle\theta_{n,c.m.}\rangle$ and the corresponding values for A are listed in table 4, together with the neutron beam polarization P_n, evaluated with eq. (9), and averaged over the angular range of the polarimeter. The values for P_n are the same as shown in fig. 1. The errors on P_n given in table 4 are only statistical. They do not contain uncertainties from the used values of A. In fig. 8, A_{00n0} is shown as a function of the energy, together with experimental data from other experiments. This shows that the values used for A represent the experimental situation very well.

References

1) C. Lechanoine-Leluc, F. Lehar, P. Winternitz and J. Bystricky, J. de Phys. **48** (1987) 985
2) R.A. Arndt, Phys. Rev. **D37** (1988) 2665
3) R. Binz, J. Franz, N. Hamann, R. Peschina, E. Rössle, H. Schmitt, G. Gaillard, E. Heer, R. Hess, C. Lechanoine-Leluc, D. Rapin, B. van den Brandt, M. Daum, A. Konter, S. Mango and P.A. Schmelzbach, np elastic scattering - Proposal for an experiment with polarized neutrons in the NA1 area at SIN, Internal Report SIN Proposal R-87-12, 1, 1987
4) M. Daum, R. Hess and E. Rössle, Feasibility study for a polarized neutron beam from the E-target at SIN, Internal Report SIN Proposal R-85-03, 1985
5) J. Franz, N. Hamann, R. Peschina, E. Rössle, H. Schmitt, H.L. Woolverton, R. Hess, C. Lechanoine-Leluc, P. Rapin, Ph. Demierre, M. Daum, J. Jaccard, J.A. Konter, S. Mango and B. van den Brandt, Experiments with polarized neutrons in nE1 - spin correlations and total cross sections, Internal Report SIN Proposal R-86-14, 1, 1986

6) R. Binz, J. Franz, N. Hamann, R. Peschina, R. Rössle, H. Schmitt, G. Gaillard, R. Hess, C. Lechanoine-Leluc, D. Rapin, Ph. Demierre, B. van den Brandt, M. Daum, J.A. Konter, S. Mango and P.A. Schmelzbach, Measurement of the spin dependent total cross sections in the neutron-proton scattering $\Delta\sigma_L$ and $\Delta\sigma_T$, Internal Report Addendum to Proposal R-86-14, 1, 1986
7) R. Binz, R. Büchle, M. Daum, J. Franz, G. Gaillard, N. Hamann, R. Hess, S. Jaccard, F. Lehar, C. Lechanoine-Leluc, A.C. Letestu, R. Peschina, D. Rapin, E. Rössle, P.A. Schmelzbach, H. Schmitt, R. Todenhagen and H.L. Woolverton, Phys. Lett. **B231** (1989) 323
8) J. Bystricky, F. Lehar and P. Winternitz, J. de Phys. **39** (1978) 1
9) V. Grundies, J. Franz, E. Rössle and H. Schmitt, Phys. Lett. **B158** (1985) 15
10) P.W. Lisowski, R.E. Shamu, G.F. Auchampaugh, N.S.P. King, M.S. Moore, G.L. Morgan and T.S. Singleton, Phys. Rev. Lett. **49** (1982) 255
11) M. Kleinschmidt, Th. Fischer, G. Hammel, W. Hürster, K. Kern, L. Lehmann, E. Rössle and H. Schmitt, Z. Phys. **A298** (1980) 253
12) S. Jaccard, J. Phys. Soc. (Japan) **55** (1986) 1062
13) P.A. Schmelzbach, D. Singy, W. Grüebler and W.Z. Zhang, Nucl. Instr. Meth. **A251** (1986) 407
14) R. Balzers, R. Henneck, Ch. Jacquemart, L. Lang, F. Nessi-Tedaldi, T. Roser, M. Simonius, W. Haeberli, S. Jaccard, W. Reichart and Ch. Weddigen, Phys. Rev. **C30** (1984) 1409
15) Saclay-Geneva phase shift solution 1990, C. Lechanoine-Leluc, private communication
16) C.D. Lac, J. Ball, J. Bystricky, J. Derégel, F. Lehar, A. de Lesquen, L. van Rossum, J.M. Fontaine, F. Perrot, P. Bach, G. Gaillard, R. Hess, Ph. Sormani, R. Binz, R. Peschina, E. Rössle, H. Schmitt, V. Ghazikhanian and C.A. Whitten, 8th Int. Symp. on high energy spin physics, Minneapolis, MN, USA, Sept. 12-17, 1988
17) F. Perrot, H. Azaiez, J. Ball, J. Bystricky, P. Chaumette, Ph. Chesny, J. Derégel, J. Fabre, J.M. Fontaine, J. Gosset, F. Lehar, W.R. Leo, A. De Lesquen, C.R. Newsom, Y. Onel, A. Penzo, L. van Rossum, T. Siemiarczuk, J. Vrzal, C.A. Whitten and J. Yonnet, Nucl. Phys. **B278** (1986) 881
18) I.P. Auer, W.R. Ditzler, D. Hill, H. Spinka, N. Tamura, G. Theodosiou, K. Toshioka, D. Underwood, R. Wagner and A. Yokosawa, Phys. Rev. Lett. **46** (1981) 1177
19) J. Bystricky, C. Lechanoine-Leluc and F. Lehar, J. de Phys. **48** (1987) 199
20) R.A. Arndt, J.S. Hyslop III and L.D. Roper, Scattering analysis interactive dial-in (SAID) system, solution SM89, as described in Phys. Rev. **D35** (1987) 128
21) T. Heuduk (1990), private communication